





Si and Sn doping of ϵ -Ga₂O₃ layers

Cite as: APL Mater. 7, 031114 (2019); doi: 10.1063/1.5050982

Submitted: 4 August 2018 • Accepted: 25 February 2019 •

Published Online: 26 March 2019



A. Parisini,¹  A. Bosio,¹ V. Montedoro,^{1,2} A. Correrri,¹ A. Lamperti,³  M. Bosi,²  G. Garulli,¹ S. Vantaggio,¹ and R. Fornari^{1,2} 

AFFILIATIONS

¹Department of Mathematical, Physical and Computer Sciences, University of Parma, Viale delle Scienze 7/A, 43124 Parma, Italy

²Institute of Materials for Electronics and Magnetism (IMEM-CNR), Viale delle Scienze 37/A, 43124 Parma, Italy

³Institute for Microelectronics and Microsystems, CNR-IMM Agrate Unit, Via Camillo Olivetti 2, 20864 Agrate Brianza (MB), Italy

ABSTRACT

Low resistivity *n*-type ϵ -Ga₂O₃ epilayers were obtained for the first time either by adding silane to the gas phase during the metal organic vapour phase epitaxy deposition or by diffusing Sn in nominally undoped layers after the growth. The highest doping concentrations were few 10¹⁸ cm⁻³ and about 10¹⁷ cm⁻³ for Si and Sn doping, with corresponding resistivity below 1 and 10 Ω cm, respectively. Temperature dependent transport investigation in the range of 10–600 K shows a resistivity behavior consistent with the Mott law, suggesting that conduction through localized states dominates the electrical properties of Si- and Sn-doped samples. For both types of dopants, two different mechanisms of conduction through impurity band states seem to be present, each of them determining the transport behavior at the lower and higher temperatures of the measurement range.

© 2019 Author(s). All article content, except where otherwise noted, is licensed under a Creative Commons Attribution (CC BY) license (<http://creativecommons.org/licenses/by/4.0/>). <https://doi.org/10.1063/1.5050982>

Group III-sesquioxides (Ga₂O₃, In₂O₃, and their alloys) have recently attracted attention as wide-bandgap semiconductors for power devices with high breakdown voltage, short wavelength photonics, gas sensors,^{1–4} and spintronics.^{5,6} Among the five polymorphs of Ga₂O₃ (α , β , γ , δ , and ϵ), monoclinic β -Ga₂O₃ is the only one which is thermodynamically stable. It presents some advantages, such as a bandgap of nearly 5 eV, transparency up to the UV-C range, and possibility to grow large crystals from the melt,^{7,8} but it also has some disadvantages such as the monoclinic structure, prone to easy cleavage, and the relatively large anisotropy of thermal, vibrational, and optical properties.^{9–12} On the other hand, the anisotropy of the electrical properties is quite limited,^{13–15} with a nearly scalar effective electron mass^{16,17} and negligible off-diagonal elements of the conductive tensor.^{14,18}

ϵ -Ga₂O₃ is believed to be the second most stable polymorph and was grown as single-phase layers on GaN, AlN, and β -Ga₂O₃ substrates by halide vapour phase epitaxy¹⁹ or Metal Organic Vapour Phase Epitaxy (MOVPE), on *c*-sapphire²⁰ and 6H-SiC.²¹ The energy gap of the ϵ polymorph is about 4.6 eV,²² which is close to that of the β phase. The transition to the β phase was observed to occur at temperatures above 850 °C.²³ Such properties allow the application of this polymorph in conventional devices, such as UV detectors.²²

ϵ -Ga₂O₃ is composed of domains (size: 5–10 nm, separated by 120° twins) with an orthorhombic structure (space group Pna2₁) as recently demonstrated by High-Resolution Transmission Electron Microscopy (HR-TEM).²⁴ The crystal structure of Ga₂O₃ layers consists of an ABAC oxygen close-packed stacking, where Ga atoms occupy octahedral and tetrahedral sites in between. Anti-phase boundaries are often found inside the domains. ϵ -Ga₂O₃ layers were seen to exhibit a good match to *c*-oriented Al₂O₃ and few more hexagonal substrates. Indeed, the 120° domain arrangement well supports a pseudo-hexagonal symmetry.

So far, electrical properties of ϵ -Ga₂O₃ were studied only for the as-grown nominally undoped material deposited by MOVPE on sapphire. The resistivity at RT was so high that transport measurements were difficult, even when using an electrometer-based apparatus. The thermal activation energy for the dark current was estimated to be about 0.7 eV by heating the samples up to 300 °C.²²

In this work, we report for the first time on *n*-type ϵ -Ga₂O₃ doped with Si and Sn by two different methods, i.e., either by introducing silane (SiH₄) into the MOVPE reactor during the epitaxial growth or by *ex situ* Sn diffusion into nominally undoped ϵ -Ga₂O₃ films. It is shown that room temperature (RT) resistivity drops below 1 and 10 Ω cm upon Si- and Sn-doping, respectively, while the

resistivity behavior with temperature is consistent with the transport through localized states (impurity band conduction).

The nominally undoped films studied in this work were grown by MOVPE at 60 mbar on 2" *c*-oriented sapphire substrates heated at 600–610 °C; trimethylgallium (TMG) and ultrapure water were used as precursors, stored in dedicated stainless steel bubblers kept at 1 °C and 30 °C, respectively. The ratio between the partial pressures of the reagents in the growth chamber ($p_{\text{H}_2\text{O}}/p_{\text{TMG}}$) was about 150. Ultrapure H_2 was used as a carrier gas, with a flow of 2000 SCCM. The films were transparent and smooth. X-ray investigation confirmed the good quality of the films, resulting in a pure (single) ϵ phase, as in previous investigations.^{20,23}

Silicon doping was obtained by adding silane to the gas phase during the growth. To this extent, a diluted mixture of 0.05% SiH_4 in pure H_2 was injected into the growth chamber to give an overall 0.005 SCCM flow of silane. Due to the horizontal configuration of the growth chamber and the absence of substrate rotation, the samples show a thickness gradient along the flow direction because of progressive precursor depletion in the gas phase. For the same reason, and for the strong tendency of SiH_4 to react with oxygen, we also expect a gradient in the Si doping level. The doped samples also presented some hazy regions, outside the main precursor stream, never observed in undoped films. Such poor-quality areas were excluded from the electrical studies. As a reproducibility test, several growth runs were repeated under the same conditions. A systematic study to optimize the growth conditions in order to mitigate the effect of the precursor gradient is in progress. For the electrical investigation, small samples (about 5 mm \times 5 mm) were cut from the mirror-like zone of each wafer.

The Sn-doping was obtained by depositing a thin SnO_x ($x < 2$) layer on top of nominally undoped 10 \times 10 mm² ϵ - Ga_2O_3 samples. The deposition was made at RT by reactive sputtering from a Sn metallic target. Thermal annealing at 600 °C for 2 or 4 h in vacuum was performed to produce Sn diffusion through the ϵ - Ga_2O_3 film. A selective etching ($\text{HF}:\text{HNO}_3 = 50:50$) was then used to remove the residual SnO_x from the surface. Ga_2O_3 epilayers with thickness between 0.3 and 1 μm were investigated. The electrical properties of different samples cut from an undoped wafer submitted to Sn sputtering and annealing showed very comparable properties, which demonstrates the reproducibility of the diffusion procedure.

To rule out any surface effects, also some Si-doped samples were etched on $\text{HF}:\text{HNO}_3 = 50:50$, similar to Sn-doped samples. However, no differences were observed in comparison with Si-doped samples whose surface was simply cleaned with organic solvents. This indicates that the measured electrical properties are relevant to the bulk and that no silicon segregation takes place.

In order to test the uniformity of the Si and Sn impurity incorporation in depth, Time of Flight-Secondary Ion Mass Spectrometry (ToF-SIMS) investigation was performed on selected samples. ToF-SIMS depth profiles were performed on a dual beam ION-TOF IV instrument (ION-TOF GmbH) using Cs^+ ions with an energy of 2 keV with a current of 160 nA for sputtering an area of 300 μm \times 300 μm and Ga^+ ions with an energy of 25 keV and a current of 3.5 pA for the analysis of a 100 μm \times 100 μm area centered on the sputtered crater. For further details, see Ref. 25. During the measurements, the instrument was operating with a flooding gun for charge compensation, 200 ms pausing time between sputtering and analysis followed by 5 s sputtering time. Negative secondary ions are

collected similarly to Ref. 25 and normalized to the intensity of Al in bulk sapphire substrates.

Ti/Au double layer contacts were fabricated by sputtering-deposition on the corners of square-shaped doped samples, in order to make transport measurements by the van der Pauw method. The as-deposited contacts exhibited a nearly ohmic behavior in a relatively wide range of their I-V characteristics, even without alloying treatment. This was important in order to monitor any changes in the epilayer conductivity due to heating, as well as to exposure to light and different atmospheres. A Keithley Hall-measurement setup was employed, and a magnetic field of 0.8 T was applied for the Hall measurements. Reliability of the measurements was proved by the current-independent results. The electrical measurements were performed in vacuum and dark, in the 10–600 K temperature range, first lowering the temperature from RT to 10 K and then increasing it up to 600 K. Experimental data were not corrected for the effects of finite dimensions of the contacts. Comparable ratios between the contact and sample sides were maintained, resulting in similar corrective factors at any temperature and for all samples. Typical uncertainties on the resistivity values are of 5%; on the Hall voltage, they are of 10%.

Electrical investigation of nominally undoped samples, reported in Ref. 22, demonstrated the very high resistivity of our MOVPE ϵ - Ga_2O_3 , which prevented any RT electrical measurement. From the high temperature I-V measurements of undoped samples, the RT Fermi level was estimated to lie at least 0.7 eV below the conduction band (CB) edge. By contrast, all epitaxial layers of the present study have RT resistivity of the order of a few Ωcm , regardless of the employed doping method, for the first time demonstrating that this polymorph can be effectively doped by the same standard Sn and Si impurities used for β - Ga_2O_3 .

Figure 1 shows ToF-SIMS profiles of Si in a layer doped via SiH_4 addition, detected by collecting Si and SiO_2 secondary ions; in particular, because of the oxide matrix (i.e., Ga_2O_3), the collection of SiO_2 is favoured over the elemental Si, which explains its higher intensity. Si distribution is uniform across the film. The little bump in the profile close to the substrate/film interface is an artefact at the Ga_2O_3 /sapphire interface due to the abrupt change in the chemical matrix. It should be noted that ToF-SIMS analysis here aims at checking the Si presence and uniformity but does not provide a quantitative estimate of its chemical concentration. The ToF-SIMS investigation of Sn-diffused specimens unfortunately was not so straightforward because of mass interference and detection limit of the instrumentation. In order to confirm that the observed *n*-type conductivity of the annealed samples was actually due to in-diffusion of Sn, we repeated the anneal experiments utilizing ZnO as the capping layer instead of SnO_x . In this way, we prevented oxygen escape from the Ga_2O_3 film and also donor contamination (Zn is not acting as donor at all). After annealing completion, the ZnO layer was removed by chemical etching and electrical contacts were deposited to perform electrical measures. The resistivity of the Ga_2O_3 film was unchanged, which strongly indicates that the *n*-type conductivity in SnO_x -capped and annealed samples is due to the incorporation of Sn as a donor. Incidentally, we also observed that annealing treatments under either O_2 or N_2 atmosphere of uncapped Ga_2O_3 layers did not induce any conductivity increase.²³

In all investigated samples, the resistivity exhibits the temperature dependence typical of conduction between localized states,

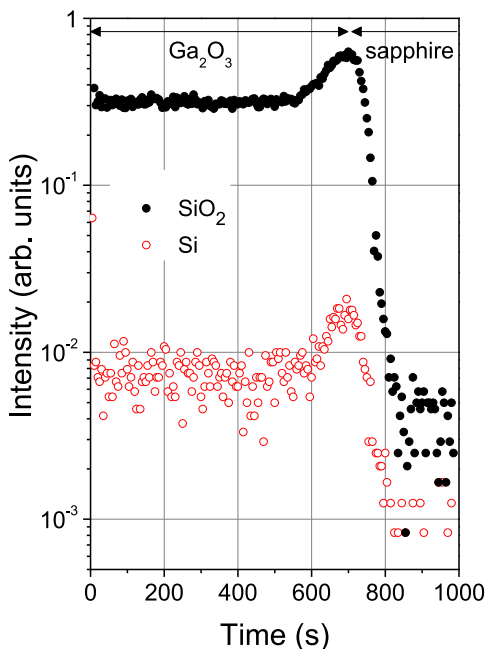


FIG. 1. ToF-SIMS profiles of Si recorded as Si and SiO₂ secondary ions, relative to sample #329 (see Table I): intensity versus sputtering time. The interface layer/substrate is reached after ~700 s of sputtering.

independently of the doping method and dopant species (Si or Sn). Moreover, the Hall voltage was detectable only in some samples and was weakly dependent on the temperature. The Hall mobility was few cm²/V s, and the corresponding Hall coefficient provided carrier densities of the order of 10¹⁷-10¹⁸ cm⁻³. Notice that, for all samples, the electrical data were derived by assuming the whole physical thickness as uniformly conductive. This assumption is fully justified for Si doping, as proved by ToF-SIMS, but may sound arbitrary in the case of Sn doping as no experimental profile of Sn diffusion is available. However, the assumption is indirectly supported by the consistency of the results obtained on Sn- and Si-doped samples.

The sign of the Hall coefficient resulted negative, which is consistent with *n*-type doping. Because Si and Sn behave as donors in ϵ -Ga₂O₃, we are confident that the sign of the Hall voltage indicates

n-type doping also for the ϵ -phase although, following Mott,²⁶ the sign and the value of the Hall voltage must be taken with precautions in the case of impurity band conduction. Angle-Resolved Photo-Electron Spectroscopy (ARPES) investigation of Si-doped films²⁷ revealed that the Fermi level (FL) approaches the CB, which provides a strong support to this conclusion. Moreover, the same ARPES study confirmed that the valence band is very flat, as recently predicted theoretically by Kim *et al.*²⁸ It is therefore to be expected that holes should give negligible contribution to conductivity owing to their extremely low mobility. All these observations concur to recognize that ϵ -Ga₂O₃ doped with Si and Sn actually exhibits *n*-type conductivity.

Figure 2 reports the data of some representative samples, doped by either Si (introduced during MOVPE) or Sn (introduced by diffusion): the same data are plotted both as an Arrhenius plot and in log-scale vs $T^{-1/4}$. The process parameters and the RT electrical data of these samples are summarized in Table I. Two Si-doped samples were grown under nominally identical growth conditions, whereas a third was grown at slightly higher temperature. Sn-sputtered samples were annealed at 600 °C for 2 and 4 h, respectively.

Clear linear trends appear only in the second plot [Fig. 2(b)], suggesting the transport dominated by variable range hopping (VRH), according to the Mott law^{26,29,30}

$$\rho(T) = \rho_0 \exp\left[\left(T_0/T\right)^{1/4}\right]. \quad (1)$$

In Eq. (1), the pre-exponential term ρ_0 represents the resistivity at infinite temperature; T_0 is a reference temperature that depends (i) on the density of the energy states in proximity of the FL, $g(\mu)$, generally assumed constant (when the electron-electron interaction is neglected)^{29,30} and (ii) on the localization radius, ξ , of the states involved in the VRH transport. This length characterizes the spatial extension of the wave-function of the electron localized at a single site. More precisely, $T_0 = C/(\xi^3 g(\mu) K_B)$,^{29,30} where K_B is the Boltzmann constant. The proportionality constant C in T_0 is an empiric dimensionless parameter that depends on the network of hopping sites assumed in the model. Here, we have taken the value $C = 8^3/9\pi \approx 18.1$, as for a 3D non-interacting electron gas and randomly distributed hopping sites (see Ref. 31 for a discussion).

In VRH, carriers jump between localized sites lying within a temperature-dependent surrounding volume (having linear dimension equal to a radius called “optimal length”). The jumps are thermally activated and characterized by a temperature-dependent

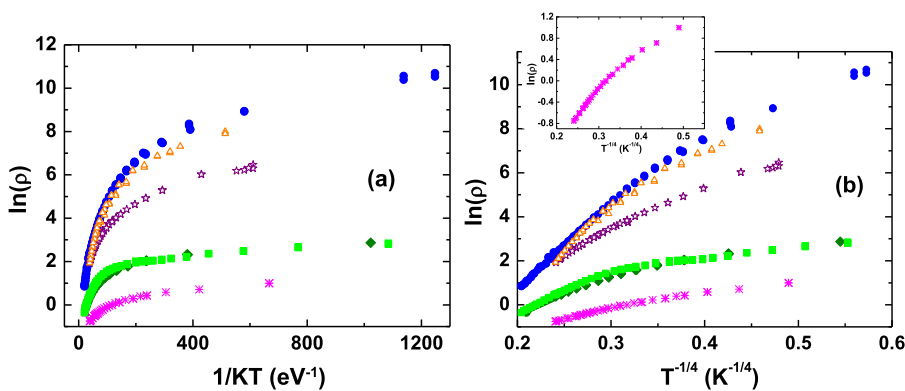


FIG. 2. (a) Arrhenius plot of the resistivity (expressed in Ω cm) of the samples of Table I. (b) Natural logarithm of the same data vs. $T^{-1/4}$ (Mott plot). In both figures, full symbols indicate the Si-doped samples (circles: #307, rhombi and squares: two pieces of #329, and asterisks: #335). Open symbols: Sn-doped samples (triangles: #317-D1 and stars: #321-D4). The inset in (b) is an enlargement of the data of #335, to better show the broken-line trend of the Mott plot.

TABLE I. Main processing parameters and RT electrical data for the investigated samples.

Sample	MOVPE growth T (°C)	Doping method	Silane flux (SCCM)	Post-sputtering annealing time (min)	Thickness (μm)	RT resistivity (Ω cm)	RT Hall mobility (cm ² /V s)	RT Hall density (cm ⁻³)
#307	600	Si-MOVPE	0.005	...	1	9.8	Not meas.	Not meas.
#321-D4	600	Sn-sputtering	...	120	0.31	6.9	3.4	2.7×10^{17}
#317-D1	600	Sn-sputtering	...	240	0.35	6.7	2.3	3.8×10^{17}
#329	600	Si-MOVPE	0.005	...	0.56	1.6	1.6	2.4×10^{18}
#335	610	Si-MOVPE	0.005	...	0.46	0.47	4.5	2.9×10^{18}

activation energy, $\omega_{opt} = 0.25K_B T(T/T_0)^{1/4}$, called “optimal energy.”²⁹⁻³¹ For this reason, the Arrhenius plot [Fig. 2(a)] of the same data shows continuously variable slopes.

The slopes of the linear segments of a typical “Mott plot,” instead, relate to the density of the localised states involved in VRH processes. All curves of Fig. 2(b) are clearly characterised by two slopes, which could correspond to two types of defects involved in distinct hopping processes, and in any case to two different transport regimes, each one dominating in a typical temperature range. Such a trend was observed in all investigated samples.

The data of samples #335 (most conductive, see Table I) and #307 (most resistive) were analyzed in the two transport regimes, by means of Eq. (1), in order to have quantitative estimates of material parameters. In the first case, the linear trends observed in the Mott plot have slopes $10.8 \pm 0.1 \text{ K}^{1/4}$ and $5.2 \pm 0.2 \text{ K}^{1/4}$, respectively, at high temperature (HT) and low temperature (LT), corresponding to the solid lines superimposed to the experimental data in the inset of Fig. 2. For the second sample, the slopes resulted are of $39.2 \pm 0.1 \text{ K}^{1/4}$ (HT) and of $19.0 \pm 0.2 \text{ K}^{1/4}$ (LT): the fits of these data are shown in Fig. 3.

If the localization radius ξ is reasonably taken of the order of the nm (e.g., 3 nm, see Ref. 31 and references therein for justification), for sample #355, a corresponding density of sites approaching

10^{19} cm^{-3} is obtained, for the HT and LT conduction regimes, from the product $g(\mu)\omega_{opt}$, both at RT and at $T = 25 \text{ K}$. The same calculation repeated for sample #307 gives densities of a few 10^{17} cm^{-3} . In principle, when VRH transport occurs, the density of sites derived from the slope of a “Mott plot” corresponds to the concentration of localized states involved in the transport. Actually, the density extracted from the Mott slopes of Fig. 3 well matches the RT Hall carrier concentration (related to the net donor density) expected for sample #307. The density of localized sites for sample #335 was slightly higher than the RT Hall density. This is reasonable because the density of the available sites must exceed the carrier density and also points at a significant compensation. Similarly, looking at the behaviors of Fig. 2 and the data of Table I, instead, one can deduce that #307 must have a concentration of donors lower than the Sn-doped samples, therefore lower than $3 \times 10^{17} \text{ cm}^{-3}$. The consistency of Hall and VRH densities for all samples supports the proposed transport mechanism.

Lower slopes are indeed observed in the samples with lower resistivity, likely owing to the higher density of sites involved in the hopping transport. The consistency between resistivity, Hall density, and slope of the Mott plots, for Sn-diffused and Si-doped epilayers, strongly points at VRH as dominant in both sets of samples. Other investigated samples, not shown here, also exhibited a behavior coherent with this picture.

Compensation is expected to play a role in VRH. Actually, compensating acceptors may have a double function, namely, trap electrons and increase the concentration of empty donors. Furthermore, a high density of point defects, i.e., lattice disorder, is expected to influence the energy broadening of the impurity band.

A doping level of a few 10^{17} cm^{-3} was generally obtained in Sn-diffused samples, one order of magnitude lower than in the most heavily Si-doped samples. This might explain the difficulty in revealing a net profile for the Sn-containing species in Sn-diffused Ga_2O_3 films. In-plane uniformity was generally good in the Sn-diffused samples.

A possible explanation for the two slopes of the Mott plots considers that donor impurities are substitutional to Ga atoms in $\epsilon\text{-Ga}_2\text{O}_3$ as they do in $\beta\text{-Ga}_2\text{O}_3$. However, in $\epsilon\text{-Ga}_2\text{O}_3$, Ga has three non-equivalent sites, either octahedrally or tetrahedrally coordinated. It is reasonable to assume that substitution of Ga atoms in these two coordinations will produce at least two different energy states, and ultimately two different state densities. Also, the formation of complex defects with energy different

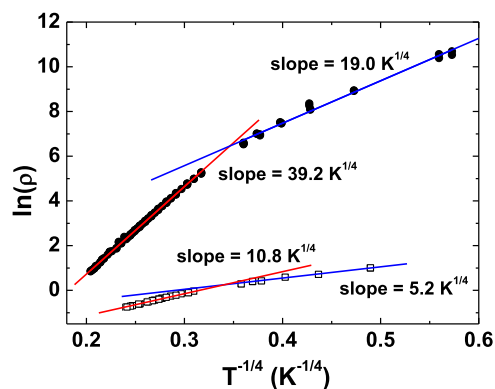


FIG. 3. Symbols: logarithm of the resistivity data (in Ω cm) vs. $T^{-1/4}$ (Mott plot) of sample #307 (full circles) and of sample #335 (open squares). Lines: linear fits of the data. Because $\ln \rho(T) = \ln \rho_0 + (T_0/T)^{1/4}$, any linear trend in the Mott plot has a slope equal to $T_0^{1/4}$.

from the one expected for Si(or Sn)-on-Ga sites cannot be excluded.

Unfortunately, the VRH data do not permit to localize the energy position of the impurity bands with respect to the conduction band (CB) or valence band edge. We can only give information on the bandwidth of the localized states *around the Fermi level* that are involved in transport (optimal energy). This width is related to the slope of the *Mott plot*

$$w_{opt} = \frac{K_B T}{4} \left(\frac{T_0}{T} \right)^{1/4} = \frac{K_B T^{3/4}}{4} \times slope. \quad (2)$$

In sample #307, the optimal energy is about 0.06 eV (HT-slope) at RT; at 25 K, it is about 0.005 eV (LT-slope).

Preliminary data from parallel ARPES investigations²⁸ carried out on one of the samples tested in the present work (#329) suggest that the CB is not populated and that at RT, the FL lies about 0.21 eV below the CB. This result is consistent with transport through a band of localized states, without intervention of free carriers, at least up to a moderate temperature of 600 K ($K_B T \approx 50$ meV). The FL position estimated by ARPES in any case confirms that ϵ -Ga₂O₃ was successfully doped as it is much closer to the CB than previously observed in undoped films.²²

Because Si and Sn in β -Ga₂O₃ behave as shallow donors (about 30 meV, e.g., ionised at RT, see Refs. 13 and 16), it is not clear why in the case of the ϵ phase such shallow levels could not be observed. As mentioned above, the deeper energy states might be connected with complex defects. A distorted lattice configuration could introduce a central cell correction to the energy state and make it deeper.

Doping-related structural disorder might be a second possible cause of electron wave-function localization. Actually, previous cathode-luminescence investigation²² and the mentioned ARPES experiments²⁸ on samples from the same series indicate the presence of families of deep states into the gap, which could be connected with structural disorder. Accurate TEM studies are necessary in order to assess the degree of disorder and eventually account for deep state or complex formation in doped materials.

To conclude, ϵ -Ga₂O₃ layers grown by MOVPE with *n*-type conductivity were obtained for the first time. Two methods were employed to introduce the donors, i.e., silane addition to the gas phase during the epitaxial growth and post-growth diffusion of Sn. SiH₄ doping results in carrier concentrations of few 10¹⁸ cm⁻³ and resistivity down to 0.5 Ω cm, while Sn diffusion gives carrier concentration in the range of 10¹⁷ cm⁻³ and resistivity of few Ω cm. ToF-SIMS investigation evidenced a nearly uniform Si incorporation, while the actual Sn-diffusion profiles into ϵ -Ga₂O₃ could not be detected due to the lower Sn concentration and detection limit of the used instrument. Nevertheless, the results of electrical characterisation carried out for both types of samples are consistent with hopping of electrons between energy states localized well below the CB edge (probably around 0.2 eV at RT, as suggested by ARPES investigation). Surely these states involve the incorporated impurities, but we cannot yet provide a definitive microscopic picture of the defects, whether simple substitutional or complexes. The VRH conduction mechanism seems to dominate the transport properties in all samples and over the explored temperature range (10-600 K); however, two different regimes are established at low and high temperatures.

The authors wish to thank Dr. Enos Gombia of IMEM-CNR Institute for the help in carrying out thermal treatments and contact preparation, Dr. Mattia Mulazzi for preliminary results of photoelectron spectroscopy, Dr. Davide Calestani for use of his chemical lab and etching facilities, and Professor Maura Pavesi and Professor Andrea Baraldi for useful discussions.

REFERENCES

- S. J. Pearton, J. Yang, P. H. Cary, F. Ren, J. Kim, M. J. Tadjer, and M. A. Mastro, *Appl. Phys. Rev.* **5**, 011301 (2018).
- J. Y. Tsao, S. Chowdhury, M. A. Hollis, D. Jena, N. M. Johnson, K. A. Jones, R. J. Kaplar, S. Rajan, C. G. Van de Walle, E. Bellotti, C. L. Chua, R. Collazo, M. E. Coltrin, J. A. Cooper, K. R. Evans, S. Graham, T. A. Grotjohn, E. R. Heller, M. Higashiwaki, M. S. Islam, P. W. Juodawlkis, M. A. Khan, A. D. Koehler, J. H. Leach, U. K. Mishra, R. J. Nemanich, R. C. N. Pilawa-Podgurski, J. B. Shealy, Z. Sitar, M. J. Tadjer, A. F. Witulski, M. Wraback, and J. A. Simmons, *Adv. Electron. Mater.* **4**, 1600501 (2018).
- S. I. Stepanov, V. I. Nikolaev, V. E. Bougrov, and A. E. Romanov, *Rev. Adv. Mater. Sci.* **44**, 63 (2016).
- M. Higashiwaki, K. Sasaki, A. Kuramata, T. Masui, and S. Yamakoshi, *Phys. Status Solidi A* **211**, 21 (2014).
- J. M. D. Coey, M. Venkatesan, and C. B. Fitzgerald, *Nat. Mater.* **4**, 173 (2005).
- A. M. H. R. Hakimi, M. G. Blamire, S. M. Heald, M. S. Alshammari, M. S. Alqahtani, D. S. Score, H. J. Blythe, A. M. Fox, and G. A. Gehring, *Phys. Rev. B* **84**, 085201 (2011).
- Y. Tamm, P. Reiche, D. Klimm, and T. Fukuda, *J. Cryst. Growth* **220**, 510 (2000).
- A. Kuramata, K. Koshi, S. Watanabe, Y. Yamaoka, T. Masui, and S. Yamakoshi, *Jpn. J. Appl. Phys., Part 2* **55**, 1202A2 (2016).
- N. Ueda, H. Hosono, R. Waseda, and H. Kawazoe, *Appl. Phys. Lett.* **71**, 933 (1997).
- F. Ricci, F. Boschi, A. Baraldi, A. Filippetti, M. Higashiwaki, A. Kuramata, V. Fiorentini, and R. Fornari, *J. Phys.: Condens. Matter* **28**, 224005 (2016).
- Z. Guo, A. Verma, X. Wu, F. Sun, A. Hickman, T. Masui, A. Kuramata, M. Higashiwaki, D. Jena, and T. Luo, *Appl. Phys. Lett.* **106**, 111909 (2015).
- M. D. Santia, N. Tandon, and J. D. Albrecht, *Appl. Phys. Lett.* **107**, 041907 (2015); Erratum **109**, 049901 (2016).
- K. Irmscher, Z. Galazka, M. Pietsch, R. Uecker, and R. Fornari, *J. Appl. Phys.* **110**, 063720 (2011).
- Y. Kang, K. Krishnaswamy, H. Peelaers, and C. G. Van de Walle, *J. Phys.: Condens. Matter* **29**, 234001 (2017).
- M. H. Wong, K. Sasaki, A. Kuramata, S. Yamakoshi, and M. Higashiwaki, *Jpn. J. Appl. Phys., Part 2* **55**, 1202B9 (2016).
- J. B. Varley, J. R. Weber, A. Janotti, and C. G. Van de Walle, *Appl. Phys. Lett.* **97**, 142106 (2010).
- E. G. Villora, K. Shimamura, Y. Yoshikawa, K. Aoki, and N. Ichinose, *J. Cryst. Growth* **270**, 420 (2004).
- A. Parisini and R. Fornari, *Semicond. Sci. Technol.* **31**, 035023 (2016).
- Y. Oshima, E. G. Villora, Y. Matsushita, S. Yamamoto, and K. Shimamura, *J. Appl. Phys.* **118**, 085301 (2015).
- F. Boschi, M. Bosi, T. Berzina, E. Buffagni, C. Ferrari, and R. Fornari, *J. Cryst. Growth* **443**, 25 (2016).
- X. Xia, Y. Chen, Q. Feng, H. Liang, P. Tao, M. Xu, and G. Du, *Appl. Phys. Lett.* **108**, 202103 (2016).
- M. Pavesi, F. Fabbri, F. Boschi, G. Piacentini, A. Baraldi, M. Bosi, E. Gombia, A. Parisini, and R. Fornari, *Mater. Chem. Phys.* **205**, 502–507 (2018).
- R. Fornari, M. Pavesi, V. Montedoro, D. Klimm, F. Mezzadri, I. Cora, B. Péc, F. Boschi, A. Parisini, A. Baraldi, C. Ferrari, E. Gombia, and M. Bosi, *Acta Mater.* **140**, 411 (2017).

- ²⁴I. Cora, F. Mezzadri, F. Boschi, M. Bosi, M. Caplovicova, G. Calestani, I. Dódonoy, B. Pécz, and R. Fornari, *Cryst. Eng. Commun.* **19**, 1509 (2017).
- ²⁵A. Lamperti, E. Cianci, O. Salicio, L. Lamagna, S. Spiga, and M. Fanciulli, *Surf. Interface Anal.* **45**(1), 390–393 (2013).
- ²⁶N. F. Mott and E. A. Davis, *Electronic Processes in Non-Crystalline Materials* (Clarendon Press, Oxford, 1971), Chap. 2, p. 53 and Chap. 6, p. 152.
- ²⁷M. Mulazzi, F. Reichmann, A. Becker, C. Wenger, A. Parisini, M. Bosi, V. Fiorentini, and R. Fornari, *APL Mater.* **7**, 022522 (2019).
- ²⁸J. Kim, D. Tahara, Y. Miura, and B. G. Kim, *Appl. Phys. Express* **11**, 061101 (2018).
- ²⁹N. F. Mott, *Metal-Insulator Transitions* (Taylor and Francis, Ltd., 1990), ISBN: 0-85066-783-6.
- ³⁰B. I. Shklovskii and A. L. Efros, *Electronic Properties of Doped Semiconductors*, Solid-State Science Vol. 45 (Springer Verlag, 1984), ISBN: 3-540-12995-2.
- ³¹A. Parisini, A. Parisini, and R. Nipoti, *J. Phys.: Condens. Matter* **29**, 035703 (2017).